Glassiness and Heterogeneous Dynamics in Dense Solutions of Ring Polymers

Davide Michieletto,[1,*] Negar Nahali,[2] and Angelo Rosa[2,†]
[1]School of Physics and Astronomy, University of Edinburgh, Peter Guthrie Tait Road, Edinburgh EH9 3FD, Scotland, United Kingdom
[2]SISSA-Scuola Internazionale Superiore di Studi Avanzati, Via Bonomea 265, 34136 Trieste, Italy
(Received 31 March 2017; published 7 November 2017)

Understanding how topological constraints affect the dynamics of polymers in solution is at the basis of any polymer theory and it is particularly needed for melts of rings. These polymers fold as crumpled and space-filling objects and, yet, they display a large number of topological constraints. To understand their role, here we systematically probe the response of solutions of rings at various densities to "random pinning" perturbations. We show that these perturbations trigger non-Gaussian and heterogeneous dynamics, eventually leading to nonergodic and glassy behavior. We then derive universal scaling relations for the values of solution density and polymer length marking the onset of vitrification in unperturbed solutions. Finally, we directly connect the heterogeneous dynamics of the rings with their spatial organization and mutual interpenetration. Our results suggest that deviations from the typical behavior observed in systems of linear polymers may originate from architecture-specific (threading) topological constraints.

DOI: 10.1103/PhysRevLett.119.197801

Introduction.—The behavior of unknotted and mutually unlinked ring polymers in dense solutions and melts is a yet unsolved issue in polymer physics [1], and it has stimulated much theoretical [2–21] and experimental [22–29] work in the last decades. One of the most elusive aspects of this problem is the interplay between topological constraints (TCs) and both structure and dynamics of the rings, which are far more intricate than in the case of linear polymers. In the latter, TCs originating from chain uncrossability [30] induce slow dynamics through the reptative motion of the chain ends [30–32] without affecting the average chain size or gyration radius R_g, which remains a random walk [33,34] and scales with the polymerization index N as $R_g \sim N^{\nu}$ with $\nu = 1/2$. In the former, rings have no ends to "reptate" [1] and global topological invariance requires that all rings remain permanently unlinked at the expense of some entropic loss [35]. Thus, TCs affect both dynamics and conformation of rings whose size is characterized by a nontrivial exponent predicted to be in the range $\nu = 1/4$ [2] and $\nu = 2/5$ [35].

In recent years, accurate computational work [6,7,12] reported evidence that in the limit of large N, $\nu \to 1/3$, according to a picture in which rings fold into crumpled conformations [36] whose compaction increases with solution density [37]. In spite of this, the surface of each ring, i.e., the fraction of contour length in contact with other chains, is "rough" and scaling as N^{β} with $\beta \lesssim 1$ [7,13,37,38]. In fact, crumpled rings do not fully segregate or expel neighboring chains from the occupied space [7], rather, they fold into interpenetrating or "threading" conformations [15,39] that are akin to interacting "lattice animals" [12] with long-range (loose) loops [21,40].

Threadings are architecture-specific TCs that uniquely populate systems of polymers whose contours display (quenched) closed loops [15,16,19,39,41] [see Fig. 1(a)]. These peculiar interactions have been shown to be instrumental for triggering "topological freezing" in solutions of rings [20]. This putative glassy state—which cannot be observed in melts of linear polymers [20]—is achieved by randomly pinning a fraction of rings, f_p, above an empirical "critical" value:

$$f_p^{\dagger}(N) = -f_N \log\left(\frac{N}{N_g}\right), \tag{1}$$

where N_g is the theoretical length required for spontaneous (i.e., $f_p \to 0$) vitrification and f_N a nonuniversal parameter [42].

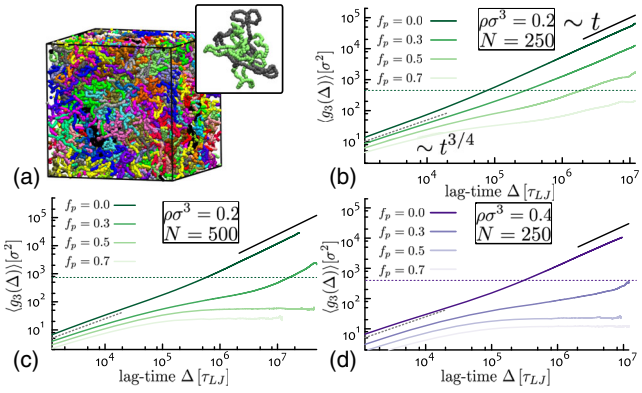

FIG. 1. Random pinning triggers slowing down and glassiness. (a) Typical melt structure for rings of $N = 250$ monomers with $f_p = 0$ and $\rho = 0.2\sigma^{-3}$. Inset: two rings isolated from the melt and showing mutual threading. (b)–(d) Mean-square displacement of rings c.m., $\langle g_3(\Delta)\rangle$ [Eq. (3)] as a function of lag time Δ (see also SM [43]). Rings display glassy behavior ($\langle g_3(\Delta)\rangle \sim \Delta^0$) for $f_p > f_p^{\dagger}$ where $f_p^{\dagger}$ decreases with both N and ρ. Dashed horizontal lines mark the mean-square ring diameters, $4\langle R_g^2\rangle$.

 © 2017 American Physical Society

Topological freezing is the consequence of the proliferation of interring constraints which depend on polymerization index N [15,18,19,41] or solution density ρ. While it has been shown that longer rings generate more TCs [18–20,41], it remains unclear how they behave if solutions become denser, rings more crumpled [37] and less space is available to threading.

Motivated by these considerations, in this Letter we study the dynamical effect of these known (threading) TCs by randomly pinning solutions of semiflexible ring polymers at different solution densities ρ. We show that the threshold pinning fraction $f_p^\dagger(\rho)$ obeys an empirical relation akin to Eq. (1) and we derive universal scaling relations for the values of N_g and ρ_g at which spontaneous ($f_p^\dagger \to 0$) glassiness is expected. We further discuss the dynamics of rings in terms of ensemble- and time-average observables and report, for the first time, numerical evidence for ergodicity breaking effects and pronounced heterogeneous non-Gaussian dynamics, even in unperturbed ($f_p = 0$) solutions.

Results.—We perform large-scale molecular dynamics simulations of dense solutions of unlinked, semiflexible ring polymers with FENE bonds, a well-established coarse-grain framework for polymer solutions [48,49]. We consider rings $N = 250$ and $N = 500$ beads long and explore monomer densities $\rho\sigma^3 = 0.1,\ 0.2,\ 0.3,\ 0.4$. For each combination of N and ρ, we run a single independent realization of the system in which a random fraction f_p of rings has been "pinned," i.e., permanently frozen in space and time, a strategy akin to that employed to study glass transition in colloids [50–52] (see Supplemental Material (SM) for details [43]).

The dynamics of a single nonfrozen ring can then be captured by the mean-square displacement of its center of mass (c.m.), $g_3(T,\Delta)$, as a function of the lag time Δ and measurement time T:

$$g_3(T,\Delta) \equiv \frac{1}{T-\Delta}\int_0^{T-\Delta} [\boldsymbol{r}_{CM}(t+\Delta) - \boldsymbol{r}_{CM}(t)]^2 dt. \quad (2)$$

The time-average displacement can be defined as $g_3(\Delta) \equiv \overline{g_3(T,\Delta)}$ while its ensemble average is defined as

$$\langle g_3(T,\Delta)\rangle \equiv \frac{1}{M_f}\sum{}' g_3(T,\Delta), \quad (3)$$

with $\sum'$ indicating that the average is performed over the set of M_f "free," i.e., not explicitly pinned, rings. Accordingly, we indicate the time- and ensemble-average displacement as $\langle g_3(\Delta)\rangle$.

Figures 1(b)–(d) and SM [43] Fig. S1 compare the behavior of $\langle g_3(\Delta)\rangle$ in response to the random pinning of different fractions f_p of rings: unperturbed solutions ($f_p = 0$) display a crossover from subdiffusive ($\langle g_3(\Delta)\rangle \sim \Delta^{3/4}$) to diffusive ($\langle g_3(\Delta)\rangle \sim \Delta$) behavior [8,13,24], whereas perturbed systems ($f_p > 0$) display reduced diffusion, the more severe the higher the value of f_p. For f_p larger than $f_p^\dagger(\rho,N)$, the average displacement remains well below one ring diameter (marked by the horizontal dashed lines) and does not diverge in time, indicating a solidlike (glassy) behavior [20]. Importantly, we observe that $f_p^\dagger(\rho,N)$ decreases with both ring length N and, unexpectedly, monomer density ρ.

In order to obtain the functional form of $f_p^\dagger(\rho,N)$, the asymptotic diffusion coefficient $D(\rho,f_p) \equiv \lim_{\Delta\to\infty}\langle g_3(\Delta)\rangle/6\Delta$ at given (N, ρ, f_p) is computed by best fit of the long-time behavior of the corresponding $\langle g_3(\Delta)\rangle$ to a linear function (see SM [43]). Figure 2(a) (also SM [43] Fig. S2) shows $D(\rho,f_p)/D_0(\rho)$—where $D_0(\rho) \equiv D(\rho,f_p=0)$—as a function of f_p. Corresponding data sets are well fitted by exponential functions $\exp(-kf_p)$ and we thus extract $f_p^\dagger(\rho,N)$ by finding their intersection with the conventional small value of 0.01 [20]. The obtained "critical" lines $f_p^\dagger(\rho,N)$ [see SM [43] Fig. S2(c)] separate regions of the parameter space (ρ,f_p) with finite (liquid) and vanishing (glassy) diffusion coefficients.

One of the main results of this work is that we find an empirical functional form $f_p^\dagger(\rho)$ akin to Eq. (1) [53], i.e.,

$$f_p^\dagger(\rho,N) = -f_\rho \log\left(\frac{\rho}{\rho_g}\right). \quad (4)$$

Thus, our data for $N = 250$ and $N = 500$ can be collapsed onto a master curve $f_p^\dagger(x = \rho/\rho_g(N))/f_\rho = -\log(x)$ with $f_\rho = 0.44 \pm 0.05$ [Fig. 2(b)]. Given that both Eqs. (1) and (4) describe the same quantity, we argue that their right-hand side must also be equal. By combining them [54] under the assumption that the only dependence on ρ is contained in N_g, the values of ρ_g and N_g for spontaneous *topological* vitrification must obey the following universal scaling relations:

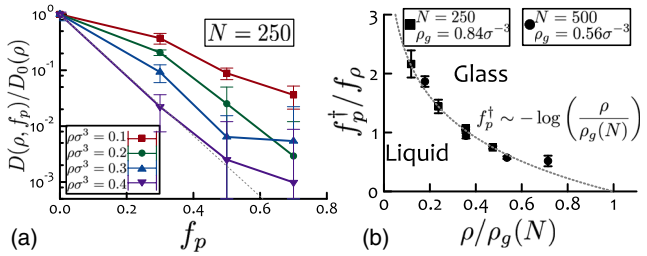

FIG. 2. Exponential slowing down and universal phase diagram. (a) $D(\rho,f_p)/D_0(\rho)$ is compatible with exponential decay (dashed line) in f_p. An arbitrarily small (0.01) value is chosen to determine the transition to glassy behavior [20]. (b) Universal master curve [$= -\log(x)$, dashed line] for $f_p^\dagger(\rho,N)/f_\rho$ as a function of $\rho/\rho_g(N)$ [see Eq. (4)] vs data (symbols) for $N = 250$ and $N = 500$ with $f_\rho(N=250) = 0.435 \pm 0.015$, $f_\rho(N = 500) = 0.445 \pm 0.05$, $\sigma^3\rho_g(N=250) = 0.84 \pm 0.05$, and $\sigma^3\rho_g(N=500) = 0.56 \pm 0.05$.

$$\rho_g(N) \sim N^{-\eta}, \qquad N_g(\rho) \sim \rho^{-1/\eta}, \tag{5}$$

with $\eta = f_N/f_\rho = 0.68 \pm 0.1$ (using $f_N = 0.30 \pm 0.05$ from Ref. [20]). This value can be compared with the one obtained by fitting the empirical $\rho_g(N)$, found to decay as $N^{-0.6}$ [see Fig. 2(b)]. Using the value of $N_g(0.1) \simeq 3500$ from Ref. [20], we can estimate the ranges $N_g(0.3) \simeq$ 520–850 and $N_g(0.4) \simeq 320$–600; these partially overlap with the parameters considered in this work and suggest that our densest and longest systems may fall close to the onset of spontaneous glassiness (see below). Importantly, Eqs. (4) and (5) provide a quantitative scaling prediction that may be tested and numerically refined through computer simulations and future experiments on randomly pinned melts of rings.

Having determined the functional form of $f_p^\dagger$ and the generic scaling of N_g and ρ_g, we now turn our attention to the role of TCs in the dynamics of single rings. We consider the distribution of $1d$ displacements Δx, $P(\Delta x) = \langle \delta(\Delta x - |x(t+\Delta) - x(t)|)\rangle$, which corresponds to the self-part of the van Hove function [55,56] at given lag time Δ. For definitiveness, we focus on the physically relevant *crossover* lag time $\Delta = \Delta_c$, defined as $\langle g_3(\Delta_c)\rangle_{f_p=0} \equiv 4\langle R_g^2\rangle$ (see dashed lines in Fig. 1).

For freely diffusing particles, the distributions of rescaled displacements $X \equiv \Delta x/\sqrt{\langle \Delta x^2\rangle}$ are expected to be described by the universal Gaussian function with zero mean and unit variance [55]. Here, instead, two additional features emerge: First, a prominence of rings with short "cagelike" displacements, identified by the region centered around $X = 0$ where $P(X)$ remains above the Gaussian. Second, the appearance of a subpopulation of rings traveling farther than the average ring, giving rise to "fat" exponential tails. Intriguingly, both are akin to features observed in generic systems of particles close to glass and jamming transitions [56]: accordingly, here they appear either in perturbed solutions of short rings [Figs. 3(b) and 3(c)] or in unperturbed systems close to the critical length $N_g(\rho)$ [see Eq. (5), Fig. 3(d), and SM [43] Fig. S3].

Thus, we claim that the non-Gaussian behavior reported here is manifestly triggered by pinning perturbations, arguably via threading TCs (see below). Further, we conjecture that threading configurations may also account for the spontaneous caging observed in unperturbed solutions at large ρ's and $N = 500$ [Fig. 3(d)]. We then argue that threadings may in general be responsible for the cagelike, non-Gaussian motion of synthetic ring polymers seen in experiments [24]. Transient threadings between rings may act as temporary cages [40], which are more long-lived the denser the solutions and the longer the rings [18–20].

In order to better understand deviations from Gaussian behavior, we now investigate time-average quantities of single ring trajectories. In Figs. 4(a) and 4(b) and SM [43]

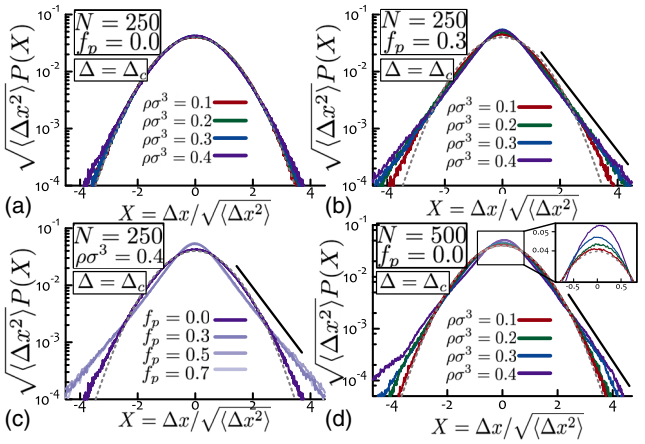

FIG. 3. Distributions of displacements are non-Gaussian. Distribution functions, $P(X)$, of $1d$ scaled displacements of the c.m. of nonpinned rings, $X \equiv \Delta x/\sqrt{\langle \Delta x^2\rangle}$, at the crossover lag time Δ_c, ($\langle g_3(\Delta_c)\rangle_{f_p=0} \equiv 4\langle R_g^2\rangle$). (a) Unperturbed solutions of short rings follow a Gaussian function with zero mean and unit variance (dashed lines). (b),(c) Perturbed solutions display caging and fat, exponential tails (solid lines). (d) Deviations from Gaussian behavior are also observed in unperturbed solutions with $N = 500$ and $\rho\sigma^3 \geq 0.3$ since $N \simeq N_g(\rho)$. Deviations become more marked as Δ increases (SM [43] Fig. S3).

Fig. S4 we report $g_3(T, \Delta_c)/\langle g_3(\Delta_c)\rangle_{f_p=0}$, i.e., the c.m. displacement of single rings at fixed lag time $\Delta = \Delta_c$ and increasing measurement time T, normalized with respect to the mean value in the unpinned case. We show that in unperturbed solutions of short polymers, any ring travels at similar speed [Fig. 4(a), $f_p = 0$] whereas, after pinning, the systems display spatial and temporal heterogeneity in the

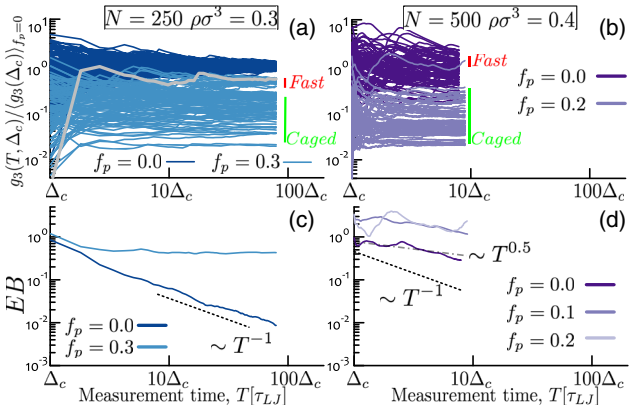

FIG. 4. Heterogeneity and ergodicity breaking. (a),(b) Representative curves for $g_3(T, \Delta_c)/\langle g_3(\Delta_c)\rangle_{f_p=0}$ at fixed lag time $\Delta = \Delta_c$ as a function of measurement time T displaying spatial and temporal (gray trace) heterogeneity. (c),(d) Corresponding ergodicity-breaking (EB) parameters [Eq. (6)]. EB $\sim T^{-1}$ marks standard diffusive processes, whereas $\sim T^0$ is a signature of ergodicity breaking. The system with $N = 500$ at the highest density $\rho\sigma^3 = 0.4$ shows weaker convergence $\sim T^{-0.5}$ even at $f_p = 0$.

trajectories which cluster into distinct fast- and slow-moving (caged) components (Fig. 4 and SM [43] Figs. S5-S6; see also cluster analysis in SM [43]). Taken together, these observations agree with the concept of permanent and transient caging due to threading TCs.

Constraints with diverging lifetimes have been shown to trigger nonergodic behavior [57]. We quantify these deviations form ergodic diffusion through the ergodicity-breaking parameter [44]

$$\mathrm{EB}(T) \equiv \frac{[\langle g_3(T,\Delta_c)^2\rangle - \langle g_3(T,\Delta_c)\rangle^2]}{\langle g_3(T,\Delta_c)\rangle^2}, \tag{6}$$

which captures how fast the single-ring trajectories $g_3(T,\Delta_c)$ narrow around the mean $\langle g_3(\Delta_c)\rangle$. For standard diffusive solutions, $\mathrm{EB}(T)$ decays as T^{-1} [44,45] whereas in nonergodic systems $\mathrm{EB} \sim T^0$ [58]. As shown in Fig. 4(c) (see also SM [43] Fig. S7) ergodicity breaking can indeed be triggered by random pinning. Remarkably, and in agreement with the predictions of Eq. (5), we observe weaker convergence to ergodicity in unperturbed solutions *only* for $N = 500$ and $\rho = 0.4\sigma^{-3}$ [Fig. 4(d)], thereby suggesting nonstandard statistics in the waiting times of diffusing rings [45,58].

Having investigated the heterogeneous dynamics of single rings, we now aim to connect the observed non-Gaussian dynamics to the spatial organization of the chains. First, one may argue [11,35] that a ring of size R_g experiences an entropic penalty proportional to the average number of overlapping neighbors $\langle m_{\mathrm{ov}}\rangle$

$$\frac{S}{k_B T} \sim \langle m_{\mathrm{ov}}\rangle \sim \frac{\rho}{N} R_g^3 \sim \rho^{\alpha}, \tag{7}$$

where we assume that [6,7,12], in the large-N limit, the number of chains in a volume R_g^3 converges to a (density dependent) constant characterized by an exponent $\alpha < 1$ [37], i.e., $R_g^3/N \sim \rho^{-(1-\alpha)}$. In Eq. (7), $\langle m_{\mathrm{ov}}\rangle$ is defined as the average number of chains whose c.m. is within $1.4\langle R_g\rangle$ [18] from any other ring. We find that $\lim_{N\to\infty}\langle m_{\mathrm{ov}}\rangle$ is weak on N and $\alpha \simeq 0.60$–0.74 [Fig. 5(a)]. Importantly, Eq. (7) implies that higher monomer densities lead to a larger number of overlapping neighbors [37] and, in turn, larger entropic penalties [35], thereby driving more compact conformations. Counterintuitively, results from Figs. 1 and 2 suggest that denser systems are more susceptible to random pinning, and display glassy behavior at *lower* values of f_p.

This apparent contradiction can be reconciled by resorting to the following picture. We consider rings as nodes of an abstract network, where a link between two nodes indicates that the corresponding rings overlap for a total time longer than half of the overall simulation run time. Two examples of networks are given in Fig. 5(b) and SM [43] Fig. S8, where nodes have been colored according to their diffusion coefficients. These show that slow or caged rings are connected (overlap persistently) either with other

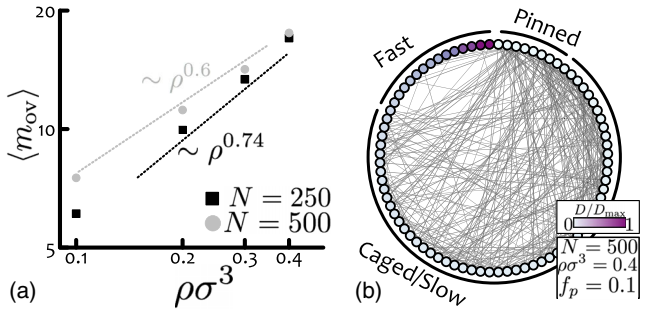

FIG. 5. Slowing down of persistently overlapping rings. (a) Average number of overlapping chains per ring, $\langle m_{\mathrm{ov}}(\rho)\rangle$. Dashed lines correspond to the fitted power-law behaviors (see Table SII in SM [43]). (b) Abstract network representation: nodes (representing rings) are color coded and arranged clockwise according to their relative diffusion coefficients, $D/D_{\max}$. Edges are drawn only if the nodes have been overlapping for more than 50% of the total run time. Notice that while all rings display the same m_{ov} at any time, slow-moving and caged nodes display larger degrees indicating more persistent overlaps. In contrast, fast rings show little or no long-time overlaps (see also SM [43] Fig. S8).

slow or caged rings or with pinned ones, whereas fast rings have virtually zero degree. The network thus directly connects the static conformations to the dynamic properties of the rings, by showing that overlapping rings reciprocally slow down owing to their mutual TCs.

To obtain a quantitative estimation of how TCs affect the dynamics of rings, we approximate the network as a Bethe lattice [32] of coordination $\langle m_{\mathrm{ov}}\rangle$. The maximum number of shells is

$$\bar{g} = \frac{\log\left(\frac{\langle m_{\mathrm{ov}}\rangle - 2}{\langle m_{\mathrm{ov}}\rangle}(M-1)+1\right)}{\log(\langle m_{\mathrm{ov}}\rangle - 1)}, \tag{8}$$

with M the total number of nodes. We now assume that the effect of pinning a single ring results in a "caging cascade," i.e., caging of its first neighbors with an *unknown* probability p_c, of its second neighbors with probability p_c^2, and so on, generating a fraction of trapped rings equal to f_c'. Assuming that for small f_p all pinned rings act independently on their neighbors, we obtain the total fraction of caged rings f_c as

$$f_c = f_p f_c' = f_p p_c \langle m_{\mathrm{ov}}\rangle \frac{(p_c(\langle m_{\mathrm{ov}}\rangle - 1))^{\bar{g}} - 1}{p_c(\langle m_{\mathrm{ov}}\rangle - 1) - 1}. \tag{9}$$

Interestingly, Eq. (9) links a measurable quantity (fraction of caged rings f_c) to an imposed quantity (fraction of pinned rings f_p) and, by inversion, allows us to determine the caging (or threading) probability between close-by rings p_c. In particular, Eq. (9) implies that the system becomes "critical" when $p_c = p_c^{\dagger} \equiv 1/(\langle m_{\mathrm{ov}}\rangle - 1)$, for there exists a finite fraction f_c of caged rings even in the limit $f_p \to 0$.

Combining Eqs. (8) and (9) and evaluating f_c at $f_p = 0.3$, we can numerically extract values for p_c at any given ρ (see Table SII). Interestingly, p_c increases with ρ up to where p_c is approximately given by the predicted $p_c^\dagger$ and, curiously, we find that $p_c > p_c^\dagger$ *only* in the two cases showing spontaneous deviations from Gaussian behavior ($N = 500$ and $\rho\sigma^3 \geq 0.3$).

Conclusions.—We have shown that dense solutions of semiflexible ring polymers display rich, non-Gaussian behavior under random pinning perturbations. Glassiness is observed at pinned fractions f_p larger than a critical value $f_p^\dagger(\rho, N)$, which obeys an empirical dependence on ρ similar to the one previously reported for N [Eqs. (1)–(4) and Fig. 2]. As a consequence, we obtained novel and generic scaling relations for the critical $\rho_g(N)$ and $N_g(\rho)$ marking the onset of spontaneous topological vitrification [Eq. (5)].

We have reported the first evidence of (i) ergodicity breaking in perturbed solutions of rings and (ii) nontrivial convergence towards ergodicity together with spontaneous caging (Figs. 3 and 4) in unperturbed systems at $N \simeq N_g(\rho)$. Further, we reported that upon random pinning, rings appear to cluster into components with slow or fast diffusivities corresponding to more or less persistent overlaps with other slow or pinned rings (Fig. 5). These results can be rationalized by arguing that threadings may act as transient cages which are then quenched by the random pinning protocol.

An intriguing finding of our work is that, even in the limit $f_p \to 0$, solutions of rings may deviate from standard Gaussian behavior [Figs. 3(d) and 4(d)] and display features at the onset of "topological glassiness" provided $\rho \simeq \rho_g(N)$ or $N \simeq N_g(\rho)$ [see Eq. (5) and Fig. 2]. We suggest that a topological glass may form when the probability p_c of any pinned ring to cage any of its neighbors is $\geq p_c^\dagger$, with $p_c^\dagger$ given by a simple analytical expression for networks in the Bethe lattice approximation.

We argue that the experimentally observed [24] non-Gaussian, cagelike behavior of ring polymers melts may be well reconciled within our picture. At the same time, we hope that the present work will pave the way for future experiments and investigations on randomly pinned polymer melts.

The authors thank C. Micheletti, D. Marenduzzo, and T. Sakaue for insightful remarks on the manuscript and D. Levis for interesting suggestions.

D. M. and N. N. contributed equally to this work.

*davide.michieletto@ed.ac.uk
†anrosa@sissa.it

[1] T. C. B. McLeish, Nature (London) **7**, 933 (2008).
[2] A. R. Khokhlov and S. K. Nechaev, Phys. Lett. A **112**, 156 (1985).
[3] A. Y. Grosberg, S. K. Nechaev, and E. I. Shakhnovich, J. Phys. (Les Ulis, Fr.) **49**, 2095 (1988).
[4] S. P. Obukhov, M. Rubinstein, and T. Duke, Phys. Rev. Lett. **73**, 1263 (1994).
[5] M. Müller, J. P. Wittmer, and M. E. Cates, Phys. Rev. E **61**, 4078 (2000).
[6] J. Suzuki, A. Takano, T. Deguchi, and Y. Matsushita, J. Chem. Phys. **131**, 144902 (2009).
[7] J. D. Halverson, W. B. Lee, G. S. Grest, A. Y. Grosberg, and K. Kremer, J. Chem. Phys. **134**, 204904 (2011).
[8] J. D. Halverson, W. B. Lee, G. S. Grest, A. Y. Grosberg, and K. Kremer, J. Chem. Phys. **134**, 204905 (2011).
[9] A. Rosa, E. Orlandini, L. Tubiana, and C. Micheletti, Macromolecules **44**, 8668 (2011).
[10] T. Sakaue, Phys. Rev. E **85**, 021806 (2012).
[11] T. Sakaue, Phys. Rev. Lett. **106**, 167802 (2011).
[12] A. Rosa and R. Everaers, Phys. Rev. Lett. **112**, 118302 (2014).
[13] A. Y. Grosberg, Soft Matter **10**, 560 (2014).
[14] A. Narros, C. N. Likos, A. J. Moreno, and B. Capone, Soft Matter **10**, 9601 (2014).
[15] D. Michieletto, D. Marenduzzo, E. Orlandini, G. P. Alexander, and M. S. Turner, ACS Macro Lett. **3**, 255 (2014).
[16] D. G. Tsalikis and V. G. Mavrantzas, ACS Macro Lett. **3**, 763 (2014).
[17] J. Smrek and A. Y. Grosberg, J. Phys. Condens. Matter **27**, 064117 (2015).
[18] E. Lee, S. Kim, and Y. Jung, Macromol. Rapid Commun. **36**, 1115 (2015).
[19] D. G. Tsalikis, V. G. Mavrantzas, and D. Vlassopoulos, ACS Macro Lett. **5**, 755 (2016).
[20] D. Michieletto and M. S. Turner, Proc. Natl. Acad. Sci. USA **113**, 5195 (2016).
[21] T. Ge, S. Panyukov, and M. Rubinstein, Macromolecules **49**, 708 (2016).
[22] M. Kapnistos, M. Lang, D. Vlassopoulos, W. Pyckhout-Hintzen, D. Richter, D. Cho, T. Chang, and M. Rubinstein, Nat. Mater. **7**, 997 (2008).
[23] S. Gooßen *et al.*, Phys. Rev. Lett. **113**, 168302 (2014).
[24] A. R. Brás, S. Gooßen, M. Krutyeva, A. Radulescu, B. Farago, J. Allgaier, W. Pyckhout-Hintzen, A. Wischnewski, and D. Richter, Soft Matter **10**, 3649 (2014).
[25] S. Gooßen, M. Krutyeva, M. Sharp, A. Feoktystov, J. Allgaier, W. Pyckhout-Hintzen, A. Wischnewski, and D. Richter, Phys. Rev. Lett. **115**, 148302 (2015).
[26] D. Richter, S. Gooßen, and A. Wischnewski, Soft Matter **11**, 8535 (2015).
[27] D. Vlassopoulos, Rheol. Acta **55**, 613 (2016).
[28] R. M. Robertson, S. Laib, and D. E. Smith, Proc. Natl. Acad. Sci. U.S.A. **103**, 7310 (2006).
[29] R. M. Robertson and D. E. Smith, Proc. Natl. Acad. Sci. U.S.A. **104**, 4824 (2007).
[30] M. Doi and S. F. Edwards, *The Theory of Polymer Dynamics* (Oxford University Press, New York, 1986).
[31] P.-G. de Gennes, J. Chem. Phys. **55**, 572 (1971).
[32] M. Rubinstein and R. H. Colby, *Polymer Physics* (Oxford University Press, New York, 2003).

[33] P. J. Flory, *Statistical Mechanics of Chain Molecules* (Interscience, New York, 1969).
[34] P.-G. De Gennes, *Scaling Concepts in Polymer Physics* (Cornell University Press, Ithaca, NY, 1979).
[35] M. Cates and J. Deutsch, J. Phys. (Les Ulis, Fr.) **47**, 2121 (1986).
[36] A. Grosberg, Y. Rabin, S. Havlin, and A. Neer, Europhys. Lett. **23**, 373 (1993).
[37] N. Nahali and A. Rosa, J. Phys. Condens. Matter **28**, 065101 (2016).
[38] J. D. Halverson, K. Kremer, and A. Y. Grosberg, J. Phys. A **46**, 065002 (2013).
[39] W.-C. Lo and M. S. Turner, Europhys. Lett. **102**, 58005 (2013).
[40] D. Michieletto, Soft Matter **12**, 9485 (2016).
[41] J. Smrek and A. Y. Grosberg, ACS Macro Lett. **5**, 750 (2016).
[42] We assume that the dependence on system density ρ is solely included in N_g and that f_N is a constant parameter, which may depend on microscopic details.
[43] See Supplemental Material at http://link.aps.org/supplemental/10.1103/PhysRevLett.119.197801, which includes Refs. [44–47], for details on simulations, and additional results.
[44] J.-H. Jeon, M. Javanainen, H. Martinez-Seara, R. Metzler, and I. Vattulainen, Phys. Rev. X **6**, 021006 (2016).
[45] R. Metzler, J.-H. Jeon, A. G. Cherstvy, and E. Barkai, Phys. Chem. Chem. Phys. **16**, 24128 (2014).
[46] R. Auhl, R. Everaers, G. S. Grest, K. Kremer, and S. J. Plimpton, J. Chem. Phys. **119**, 12718 (2003).
[47] S. Plimpton, J. Comp. Physiol. **117**, 1 (1995).
[48] K. Kremer and G. S. Grest, J. Chem. Phys. **92**, 5057 (1990).
[49] R. Everaers, S. K. Sukumaran, G. S. Grest, C. Svaneborg, A. Sivasubramanian, and K. Kremer, Science **303**, 823 (2004).
[50] C. Cammarota and G. Biroli, Proc. Natl. Acad. Sci. U.S.A. **109**, 8850 (2012).
[51] E. R. Weeks, Nat. Phys. **11**, 381 (2015).
[52] S. Karmakar and G. Parisi, Proc. Natl. Acad. Sci. U.S.A. **110**, 2752 (2013).
[53] The functional similarity between Eqs. (1) and (4) may be validated by noticing that "$-\log(x)$" is a simple, monotonic function of the dimensionless parameters N/N_g and ρ/ρ_g which satisfies (a) $f_p^\dagger \to 0$ for $N \to N_g$ or $\rho \to \rho_g$ and (b) $f_p^\dagger \to +\infty$ for $N \to 0$ or $\rho \to 0$; both of which must hold by definition of $f_p^\dagger$.
[54] This is because $f_N \log[N/N_g(\rho)] = f_\rho \log[\rho/\rho_g(N)]$ and then $\rho_g(N) = \rho N_g(\rho)^\eta N^{-\eta}$. Imposing that this must be valid at any ρ one obtains $\rho N_g(\rho)^\eta = \text{const}$ or $N_g(\rho) \sim \rho^{-1/\eta}$.
[55] W. Kob, C. Donati, S. J. Plimpton, P. H. Poole, and S. C. Glotzer, Phys. Rev. Lett. **79**, 2827 (1997).
[56] P. Chaudhuri, L. Berthier, and W. Kob, Phys. Rev. Lett. **99**, 060604 (2007).
[57] P. Massignan, C. Manzo, J. A. Torreno-Pina, M. F. García-Parajo, M. Lewenstein, and G. J. Lapeyre, Phys. Rev. Lett. **112**, 150603 (2014).
[58] W. Deng and E. Barkai, Phys. Rev. E **79**, 011112 (2009).